IOP Publishing Journal of Physics: Condensed Matter
J. Phys.: Condens. Matter **32** (2020) 175701 (9pp) https://doi.org/10.1088/1361-648X/ab68f4

Superconductivity and magnetism in $RbEu(Fe_{1-x}Co_x)_4As_4$

Ya-Bin Liu[1], Yi Liu[1,4], Yan-Wei Cui[1,2], Zhi Ren[2] and Guang-Han Cao[1,3]

[1] Department of Physics and Zhejiang Province Key Laboratory of Quantum Technology and Device, Zhejiang University, Hangzhou 310027, People's Republic of China
[2] School of Sciences, Westlake Institute for Advanced Study, Westlake University, Hangzhou 310064, People's Republic of China
[3] Collaborative Innovation Centre of Advanced Microstructures, Nanjing University, Nanjing 210093, People's Republic of China

E-mail: ghcao@zju.edu.cn

Received 12 October 2019, revised 13 December 2019
Accepted for publication 8 January 2020
Published 28 January 2020

Abstract

We studied the cobalt-doping effect on superconductivity and magnetism in a hole self-doped $RbEuFe_4As_4$ magnetic superconductor which shows superconductivity at $T_c = 36.5$ K and Eu^{2+}-spin ordering at $T_m = 15$ K. The Co solubility limit in $RbEu(Fe_{1-x}Co_x)_4As_4$ achieves $x = 0.21$ for the solid-state reaction at 880 °C. With increasing x, T_c decreases gradually, and superconductivity eventually disappears at $x \geqslant 0.175$. A spin-density-wave transition at $T_{SDW} = 35$–40 K is recovered for $x \geqslant 0.1$, which can be understood in terms of the hole-depletion and the disorder effects. On the other hand, T_m remains unchanged despite the Co doping and, consequently, an intriguing superconducting ferromagnet without Meissner state is realized in the range of $0.125 \leqslant x \leqslant 0.155$. Our results indicate that the Eu^{2+} spins essentially decouple with superconductivity over a wide doping range, making the coexistence of superconductivity and ferromagnetism possible in the 1144-type system.

Keywords: iron-based superconductors, magnetic superconductor, doping effect

(Some figures may appear in colour only in the online journal)

1. Introduction

The iron-based superconductors with Eu^{2+} spins sandwiched between the FeAs layers represent a new class of magnetic superconductors [1, 2]. The 122-type magnetic superconductors feature coexistence of superconductivity (SC) and Eu-spin ferromagnetism (FM) with relatively high superconducting and magnetic transition temperatures. The parent compound $EuFe_2As_2$ exhibits not only a spin-density wave (SDW) transition at $T_{SDW} = 190$ K occurring in the FeAs layer, but also an A-type antiferromagnetic (with in-plane ferromagnetism and inter-plane antiferromagnetism, as is shown in figure 1(a)) transition at 19 K in the Eu sublattice in which the Eu^{2+} spins lie flat in the basal plane [3, 4]. With a suitable chemical doping, either with P for As [5] or, with Co [6], Ru [7], Ir [8, 9], Rh [10] for Fe, SC at $T_c \gtrsim 20$ K emerges with the disappearance of SDW. Meanwhile, the Eu^{2+} spins reorient towards the crystallographic c direction [11, 12], and order *ferromagnetically* at $T_m \approx 18$ K [13–16]. Notably, no SC could be induced with Ni doping in $EuFe_2As_2$, although the SDW was completely suppressed [17].

Recently, $AEuFe_4As_4$ (A = Rb, Cs) were discovered [18–20], which supply an additional opportunity for the study of the interplay between SC and local-moment magnetism. The new magnetic superconductors exhibit a superconducting transition at $T_c = 36.5$ K (A = Rb) or 35 K (A = Cs) followed by a magnetic transition at $T_m = 15$ K (A = Rb) or 15.5 K (A = Cs). Structurally, the materials are variants of $EuFe_2As_2$ in which one of every two Eu-layers is replaced by the alkali-metal

[4] Present Address: Research Center for Smart Sensing, Zhejiang Lab, Hangzhou 311121, China

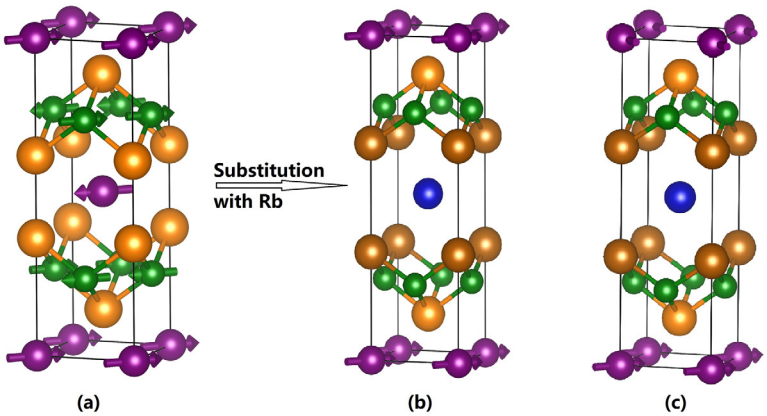

Figure 1. The crystal and magnetic structures of $EuFe_2As_2$ (a) (according to [4]) and $RbEuFe_4As_4$ (b) and (c) (according to [19, 26], respectively). The blue, purple, green, and orange balls denote Rb, Eu, Fe, and As atoms, respectively.

non-magnetic layer (see figure 1). If assuming that the magnetic interactions between Eu^{2+} spins remains unchanged, the removal of every alternating magnetic Eu-layer (being A-type antiferromagnetically ordered below T_m^{Eu} in $EuFe_2As_2$) would give rise to Eu-spin ferromagnetism with the magnetic moment lying in the *ab* plane (figure 1(b)). Indeed, the magnetization at temperatures far below the T_m saturates (under an external field of ~2 kOe) at ~6.5 μ_B/Eu [19, 21], close to the expected value of 7.0 μ_B/Eu for the Eu^{2+}-spin FM. The Mössbauer studies on $AEuFe_4As_4$ demonstrated that the Eu magnetic moments are perpendicular to the crystallographic *c* axis, and the hyperfine magnetic field at ^{151}Eu nuclei suggests ferromagnetic ordering in the Eu sublattice [22, 23]. The Eu magnetism was shown to be quasi-two dimensional [21, 24]. Upon approaching T_m, a substantial boost of the magnetic flux density along *ab* planes was observed [25]. Nevertheless, recent neutron diffraction study revealed a helical modulation with the magnetic propagation vector of $\mathbf{k} = (0, 0, 1/4)$ for the Eu-spin ordering [26] (figure 1(c)). The helical magnetic structure was explained in terms of the exchange interaction over the electromagnetic one between SC and FM [27].

Chemical doping can be a useful method to study the interplay between SC and FM. $AEuFe_4As_4$ are hole self-doped superconductors with a doping level of 0.25, i.e. the Fe formal valence is 2.25+. It is of interest to tune the system back towards the 'parent phase' in which the Fe formal valence is 2+. Unfortunately, the target non-doped compounds with a chemical formula of $ARFe_4As_4$ (*R* is a trivalent rare-earth element) could not be synthesized so far. In general, the 1144-type system tends to be a line compound in which heterovalent chemical doping at *A* site is very limited [28]. Nevertheless, the isovalent chemical substitution of Eu with Ca in $Rb(Eu_{1-x}Ca_x)Fe_4As_4$ was fully successful [29]. It was shown that, while T_m decreases gradually with the Ca doping, T_c hardly changes in the whole doping, suggesting that SC is not sensitive to the Eu-spin magnetic order. The result is not surprising because the hole-doping level does not change, and the Eu-site magnetic moments are diluted. We previously succeeded in doping extra itinerant electrons through the partial substitution of Fe with Ni [30]. The result turns out to be the opposite: T_c decreases rapidly, whereas T_m keeps unchanged, with the Ni doping in $RbEu(Fe_{1-x}Ni_x)_4As_4$. Additionally, an SDW anomaly was observed at $x \geqslant 0.05$. The insensitivity of T_m with Ni doping is explained by the first-principles calculations, which shows that the Ruderman–Kittel–Kasuya–Yosida (RKKY) interaction strength is barely changed upon the Ni doping [31].

Concerning the different doping effect of Co and Ni in $EuFe_2As_2$ [6, 17], we investigated the Co doping effect in $RbEuFe_4As_4$. Compared with Ni (Fe), Co has one less (more) 3*d* electron. Thus, Co doping is expected to introduce one extra itinerant electron per cobalt atom to compensate the self-doped holes. Our results indicate a similar effect for the Co doping, if one considers that Ni doping effectively introduces two extra itinerant electrons per nickel atom. With the Co doping, T_c decreases monotonically, and SDW ordering appears at $x \geqslant 0.1$. The SDW transition temperature shows a maximum of 40 K at $x = 0.175$. By contrast, T_m is basically invariant with the Co doping. As a result, an intriguing superconducting magnet with $T_c < T_m$ was obtained in the range of $0.125 \leqslant x \leqslant 0.155$ where there is no Meissner state because of the spontaneous magnetization in the Eu sublattice.

2. Experimental methods

Polycrystalline samples of $RbEu(Fe_{1-x}Co_x)_4As_4$ ($0 \leqslant x \leqslant 0.21$) were synthesized by a solid-state-reaction method [19, 30] using the mixtures of $RbFe_2As_2$, FeAs, EuAs, Fe, and CoAs. First, FeAs, EuAs and CoAs were prepared by reacting Fe powders (99.998%), Eu pieces (99.9%) , Co powders (99.9%) and As pieces (99.999%) at 700 °C–750 °C for 24 h. $RbFe_2As_2$ was obtained by reacting Rb (99.75%) pieces and FeAs powders at 600 °C for 24 h. Second, the stoichiometric mixtures of $RbEu(Fe_{1-x}Co_x)_4As_4$ were homogenized, pressed into pellets, and loaded in an alumina tube which was then sealed in a Ta tube. The Ta tube was further jacketed with a silica ampule filled with Ar gas. Third, the sample-loaded assembly were heated rapidly to 850 °C–900 °C in a muffle furnace. After holding for 20 h, the samples were quenched. The solid-state reaction was repeated with an intermediate grinding in order to improve the purity of the samples. Note

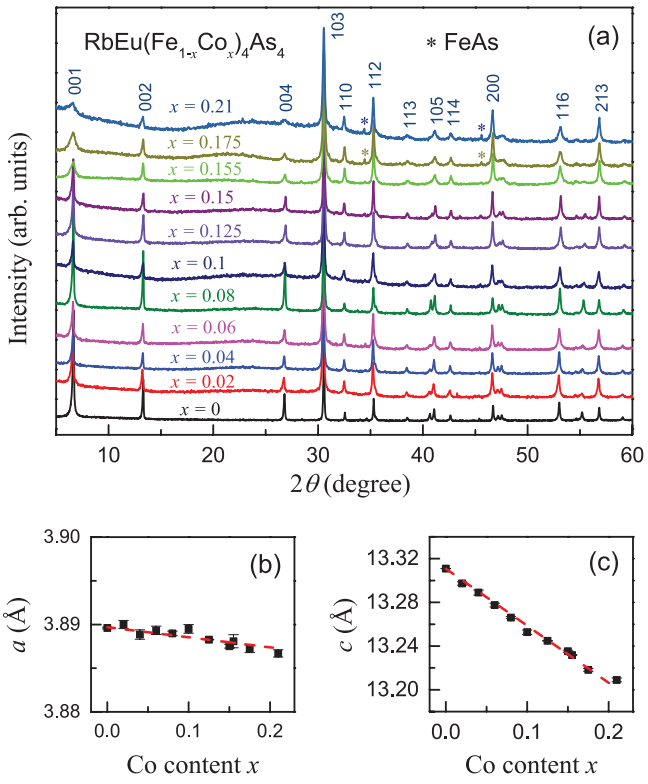

Figure 2. (a) Powder XRD patterns of the $RbEu(Fe_{1-x}Co_x)_4As_4$ samples. The lattice parameters a and c are plotted in (b) and (c), respectively, as functions of the nominal Co content. The dashed lines show the linear fit.

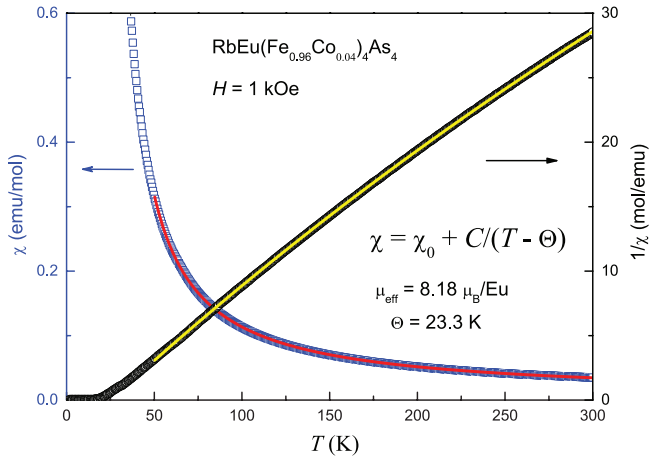

Figure 3. Temperature dependence of magnetic susceptibility for a typical sample $RbEu(Fe_{0.96}Co_{0.04})_4As_4$ under a magnetic field of 1 kOe. The reciprocal of the susceptibility (right axis) is basically linear, and the Curie–Weiss fit (solid line) yields the effective magnetic moments and the paramagnetic Curie–Weiss temperature as shown in the plot.

that most of the procedures were performed in an Ar-filled glove box with oxygen and water content less than 1 ppm.

Powder x-ray diffraction (XRD) was carried out at room temperature on a PANalytical x-ray diffractometer (Model EMPYREAN) using a monochromatic Cu-$K_{\alpha 1}$ radiation. The lattice parameters were obtained by a least-squares fit of ∼20 reflections in the range of $5° \leqslant 2\theta \leqslant 80°$. The electrical resistivity and heat capacity were measured on a quantum design physical property measurement system (PPMS-9). The magnetic properties were measured on a quantum design magnetic property measurement system (MPMS3).

3. Experimental results

The samples of $RbEu(Fe_{1-x}Co_x)_4As_4$ synthesized were first characterised by powder XRD. As shown in figure 2(a), the XRD patterns keep the same feature from $x = 0$ to 0.21, which can be well indexed on the basis of a tetragonal structure with the space group of *P*4/*mmm* (No. 123). All the samples are basically single phase, and only small amount of FeAs impurity is present for $x \geqslant 0.175$. We found that further increasing the Co nominal content beyond $x = 0.21$ led to more impurity phases. Thus the Co solubility limit is about 20% under the present synthesis conditions.

Figures 2(b) and (c) show the lattice parameters a and c as functions of the nominal Co content. One sees that both parameters decrease with the Co doping, which is primarily due to the smaller ionic size of Co^{2+} (compared with Fe^{2+}). In particular, the c parameter decreases almost linearly with x, which obeys the Vegard's law, suggesting that the actual Co-doping level is very close to the nominal one. The fact that nearly single-phase samples were synthesized in a closed container (with the least loss of the constituent elements) using the nominal composition also supports the incorporation of the dopant Co in the lattice.

Figure 3 shows the temperature dependence of magnetic susceptibility (χ) for a typical sample $RbEu(Fe_{1-x}Co_x)_4As_4$ with $x = 0.04$. The $\chi(T)$ data at high temperatures obey the Curie–Weiss law, $\chi = C/(T - \Theta) + \chi_0$, where C denotes the Curie–Weiss constant, Θ is the paramagnetic Curie–Weiss temperature, and χ_0 is the temperature-independent term. The data fitting yields $C = 8.37$ emu K mol^{-1}, $\Theta = 23.3$ K, and $\chi_0 = 0.0043$ emu mol^{-1}. The effective magnetic moment is then derived to be 8.18 μ_B per formula unit (or per Eu atom), which is close to the theoretical value of 7.94 μ_B/Eu for a free Eu^{2+} spin. The effective magnetic moment for other samples of $RbEu(Fe_{1-x}Co_x)_4As_4$ is 8.2 ± 0.3 μ_B/Eu, independent of Co doping (see table 1). The data definitely indicate the $J = S = 7/2$ state of the local moment of Eu^{2+} ions. The Θ values obtained is around 23 K, again independent of the Co doping, suggesting almost invariant ferromagnetic interactions between Eu^{2+} spins.

To demonstrate the evolutions of the superconducting and magnetic transitions, in figure 4, we plot the temperature dependence of magnetization of the $RbEu(Fe_{1-x}Co_x)_4As_4$ series samples under a low magnetic field of $H = 10$ Oe. For $x \leqslant 0.1$, a clear magnetization drop at T_c can be seen with diamagnetism (ZFC data) at lower temperatures. With increasing the Co doping to $x \geqslant 0.125$, no magnetization drop can be seen above the Eu-spin ordering temperature T_m. Nevertheless, the M_{ZFC} data of the $x = 0.125$ and 0.15 samples show an obvious slope change at 11.8 K and 9.0 K, respectively, which is probably associated with a superconducting transition. Indeed, the resistivity and specific-heat data below indicate appearance of

Table 1. List of the physical-property parameters of $RbEu(Fe_{1-x}Co_x)_4As_4$ ($0 \leqslant x \leqslant 0.21$). T_c^ρ and T_c^χ are the superconducting transition temperatures determined by electrical resistivity (midpoint) and magnetic susceptibility (onset) measurements, respectively. T_{SDW} is the spin-density-wave transition temperature. T_m and Θ are respectively the Eu-spin ordering and Curie–Weiss temperatures. P_{eff} and M_{sat} (with the unit μ_B/Eu) are the effective magnetic moment in the paramagnetic state and the ordered moment in the ferromagnetic state, respectively. H_{coe} denotes the apparent coercive field.

x	T_c^ρ (K)	T_c^χ (K)	T_{SDW} (K)	T_m (K)	Θ (K)	P_{eff}	M_{sat}	H_{coe} (Oe)
0	36.4	36.4	—	15.0	23.6	7.95	6.5	360
0.02	33.4	33.2	—	15.2	22.9	8.21	6.8	211
0.04	31.3	31.1	—	14.7	23.3	8.18	6.9	240
0.06	30.1	30.1	—	14.9	23.4	8.17	6.9	189
0.08	26.2	26.2	—	14.7	23.1	8.28	7.1	195
0.1	22.3	22.2	33.1	14.6	23.3	8.15	7.0	159
0.125	17.4	11.8	36.7	14.2	22.4	8.49	7.0	20
0.15	13.7	9.0	39.2	14.6	23.6	8.20	6.9	13
0.155	5.4	—	39.7	14.2	22.0	8.41	6.8	5
0.175	—	—	40	14.7	22.0	8.47	6.7	4
0.21	—	—	37	14.2	22.8	7.90	6.8	7

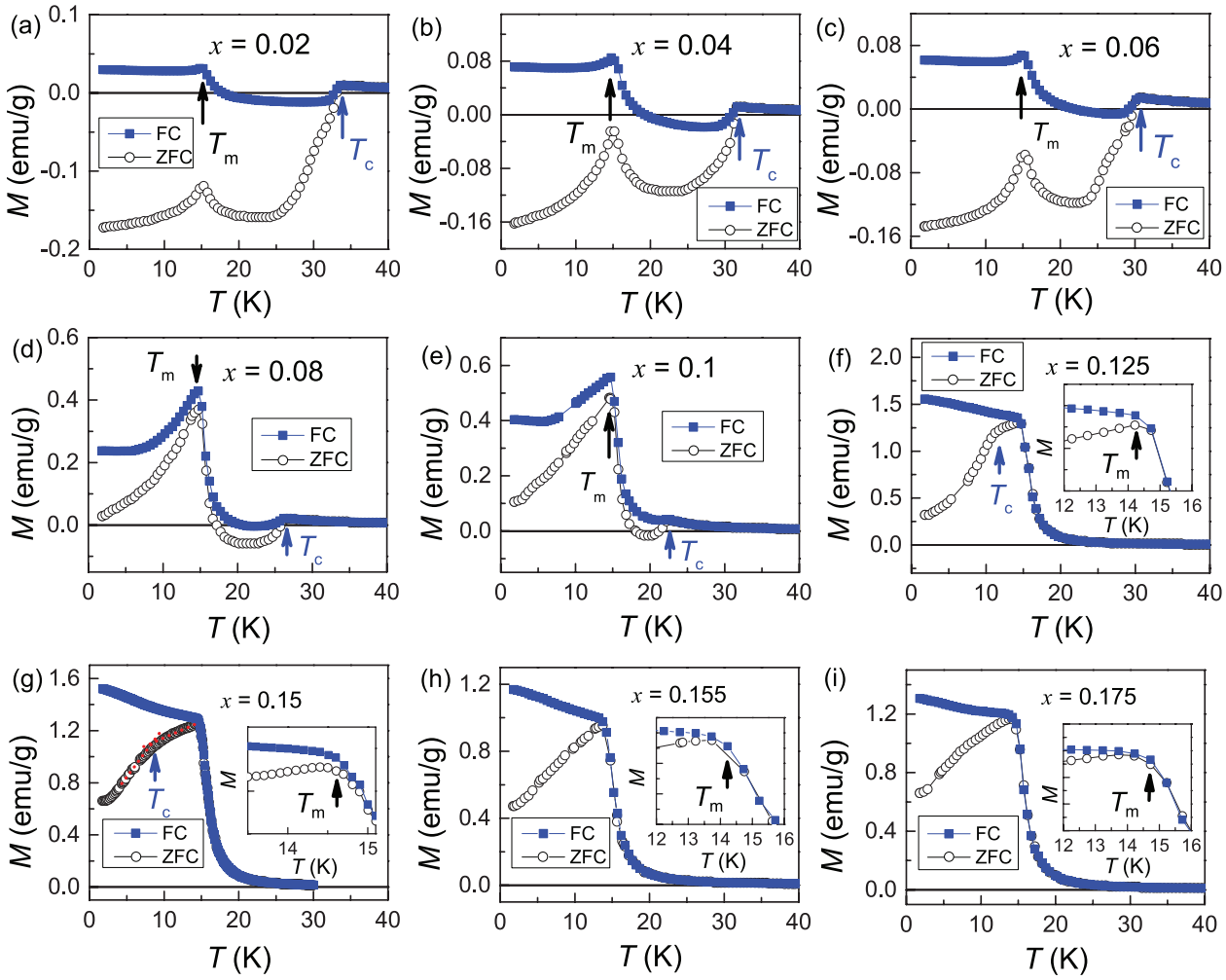

Figure 4. Temperature dependence of magnetization under $H = 10$ Oe for the $RbEu(Fe_{1-x}Co_x)_4As_4$ series samples. Panels (a)–(i) show the data for $x = 0.02$–0.175, respectively. The data were collected in a heating process with zero-field-cooling (ZFC) and field-cooling (FC) histories. T_c and T_m represent the superconducting and magnetic transition temperatures, respectively. The insets show the close-ups for the positioning of T_m.

SC for $0.125 \leqslant x \leqslant 0.155$. We will come back to this issue later on.

Unlike the gradual suppression of superconductivity, T_m basically does not change with the Co doping. The changeless T_m is actually consistent with the invariant Θ described above, although the T_m value is about 8 K lower than the Curie–Weiss temperature (see table 1). The lowered T_m reflects the quasi-two-dimensional nature of the magnetic ordering that is

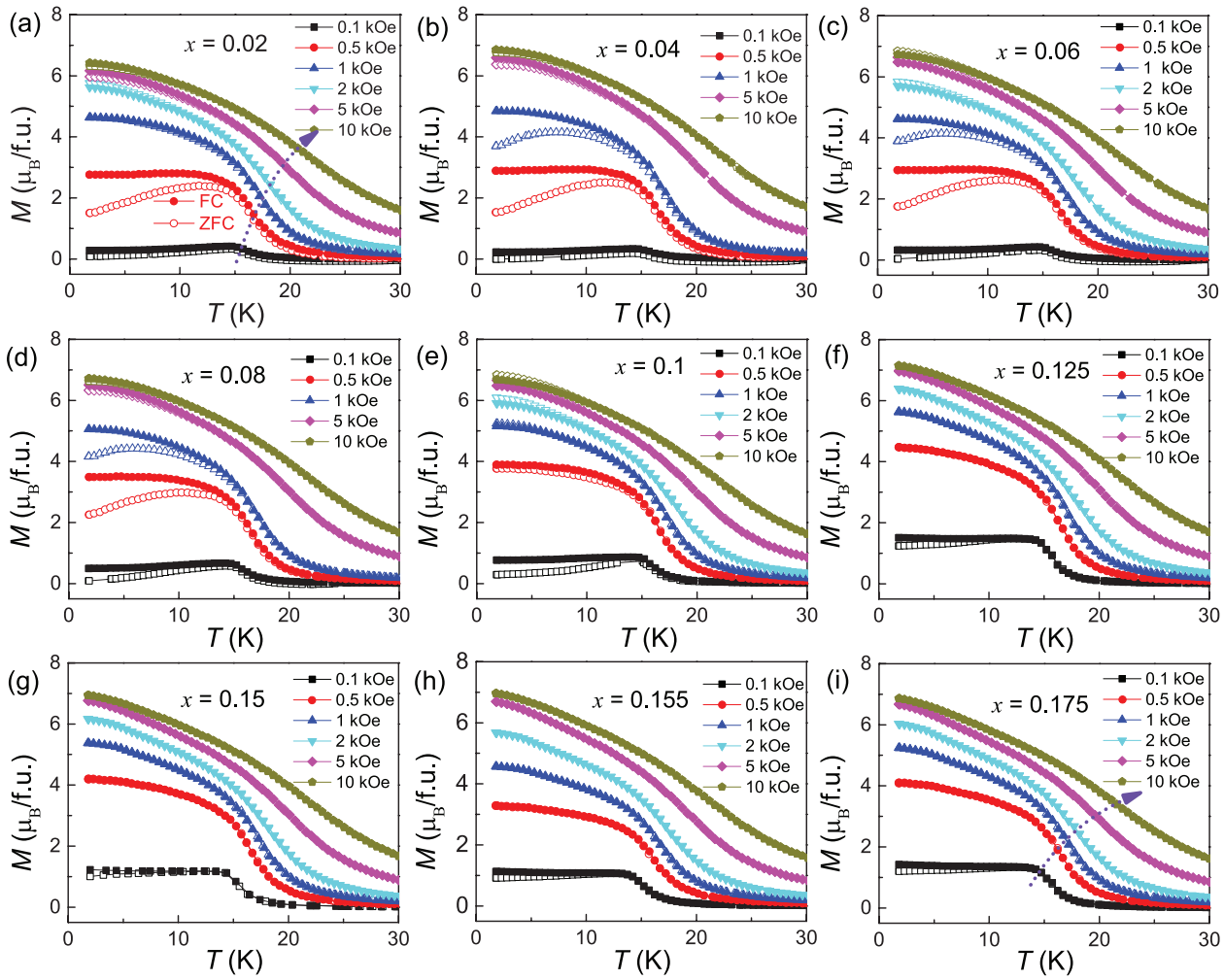

Figure 5. Temperature dependence of magnetization under different magnetic fields for $RbEu(Fe_{1-x}Co_x)_4As_4$ samples. Panels (a)–(i) show the data for $x = 0.02$–0.175, respectively. The unit of magnetization is conversed into Bohr magnetons per formula unit.

featured with very weak magnetic coupling along the c axis [19, 21, 24].

The contrasting changes between T_c and T_m with the Co doping result in a transition-temperature reversal at $x \sim 0.125$ above which T_c becomes lower than T_m. The case of $T_m > T_c$ is coined as a superconducting ferromagnet (SFM) [32], instead of a ferromagnetic superconductor (FSC) for the ordinary scenario of $T_c > T_m$. Notably, the FSC and SFM show different characteristic in the $M_{FC}(T)$ curves. For the FSC with $x \leqslant 0.1$, the $M_{FC}(T)$ data show a peak at T_m. In other words, M_{FC} *decreases* with decreasing temperature below T_m. For the SFM with $x \gtrsim 0.125$ ($T_m \gtrsim T_c$), one sees a kink, rather than a peak, at the T_m. Namely, M_{FC} *increases* with decreasing temperature below T_m, which suggests a ferromagnetic nature of the magnetic ordering [2]. Similar behaviours were observed in Ni-doped $RbEu(Fe_{1-x}Ni_x)_4As_4$ system [30]. According to the neutron diffraction study [26], the non-doped compound shows an in-plane ferromagnetism together with a helical structure between the ferromagnetic planes. This magnetic structure does not allow a net spontaneous magnetization, which naturally explains the peak-like feature at T_m. The helical magnetic structure may be due to the presence of SC [27]. If so, the magnetic ordering in the absence of SC in the SFM ($T_m > T_c$) will be a purely ferromagnetic transition, which would lead to the kink at T_m. Since the M_{FC} increases steadily with decreasing temperature, it is not expected that the helical magnetic structure would appear when SC sets in below T_m.

Here we argue that the SFM at $x \sim 0.15$ exhibits a novel superconducting ground state without Meissner regime even at zero field. The fully ferromagnetic alignment of Eu^{2+} spins generates an internal field of ~4 kOe, which is much higher than the lower critical magnetic field (c.f., the $H_{c1}^{\|ab}(0)$ value is only 0.03 kOe for the $CsCa_2Fe_4As_4F_2$ superconductor with $T_c = 30$ K [33]). Therefore, there is intrinsically no Meissner state in the SFM, according to our classification of magnetic superconductors [34]. The absence of Meissner state is similar to the case in UCoGe [35], but it is different from the case of the FSCs. In doped $EuFe_2As_2$ systems, for example, a domain Meissner state just below T_c is present and, with further cooling down below the T_m, the system evolves into a spontaneous domain vortex-antivortex state [36]. Similar phenomena are likely for the 1144-type FSCs, but the different spontaneous magnetization direction could make some

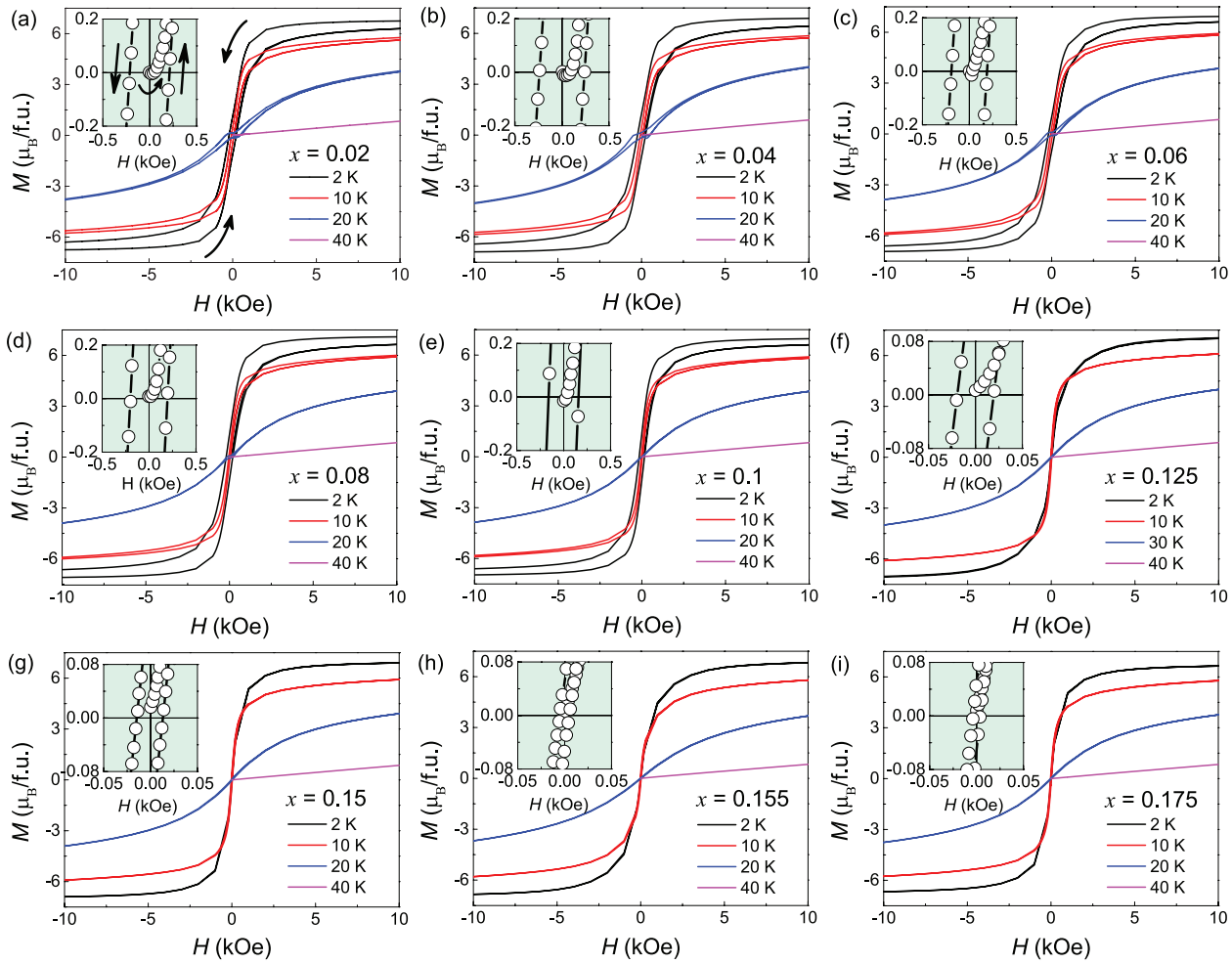

Figure 6. Isothermal magnetization of the $RbEu(Fe_{1-x}Co_x)_4As_4$ samples. Panels (a)–(i) show the data for $x = 0.02$–0.175, respectively. The insets show an expanded plot of the magnetic hysteresis at 2 K.

difference. Anyway, how SC compromises FM in the 1144-type system is an interesting issue to be investigated.

Figure 5 show the $M(T)$ data under higher magnetic fields. At $H = 0.5$ kOe, the peak in $M_{FC}(T)$ changes into a round shape, indicating a ferromagnetic transition. Meanwhile, the ferromagnetic transition temperature, T_{FM}, increases remarkably with the external field. If defined by the minimum of dM/dT, T_{FM} achieves ~23 K at 10 kOe, which is almost the same as the value of the paramagnetic Curie–Weiss temperature Θ. The magnetization at 2 K basically converges to 7.0 μ_B/Eu, consistent with the full ferromagnetic alignment of Eu^{2+} spins.

Figure 6 shows the isothermal magnetization curves for $RbEu(Fe_{1-x}Co_x)_4As_4$. Firstly, the $M(H)$ data are essentially linear at 40 K ($> T_c$ and $> T_m$), consistent with the Curie–Weiss paramagnetic state. Secondly, the $M(H)$ curves at 30 K obviously deviate from the linearity, primarily due to the exchange interactions between Eu^{2+} spins. The small hysteresis for $x \leqslant 0.06$ comes from the magnetic-flux pinning in the superconducting state. When cooled to 10 K and 2 K ($< T_m$), thirdly, the overall shape of the $M(H)$ curves is characteristic of a FM with the saturation magnetization close to the expected value of $gS = 7.0$ μ_B/Eu. At the same time, the magnetic hysteresis due to flux pinning extends to high magnetic fields for $x \leqslant 0.1$ ($T_c > T_m$). In other words, the isothermal magnetization loop is composed of two components, one is due to the ferromagnetic alignment of Eu^{2+} spins, another comes from the superconducting flux pinning. Nevertheless, in the case of $0.125 \leqslant x \leqslant 0.155$ with $T_c \lesssim T_m$, no flux pinning effect is observable as though it were not superconducting. This is because SC emerges under the spontaneous magnetization which penetrates the interior of the superconductor. Another relevant point is that the spontaneous magnetization is along the *ab* plane, and the corresponding flux-pinning force is relatively weak.

In the insets of figures 6(a)–(i), we show the close-ups of the $M(H)$ data of 2 K, from which the apparent coercive field H_{coe} can be clearly seen. The H_{coe} value is only a few Oersted for the non-superconducting ferromagnet with $x = 0.175$, indicating very soft magnetism in the material system. The increase of H_{coe} for the superconducting samples is primarily due to the flux-pinning effect, as stated above.

Figure 7 shows the temperature dependence of normalized resistivity for the $RbEu(Fe_{1-x}Co_x)_4As_4$ polycrystalline samples. While all the samples show metallic behaviours, the resistivity slope tends to decrease with increasing Co content. Consequently, the residual resistivity appears to increase with the Co doping, suggesting a disorder effect. With the Co doping, T_c decreases systematically, and SC is eventually

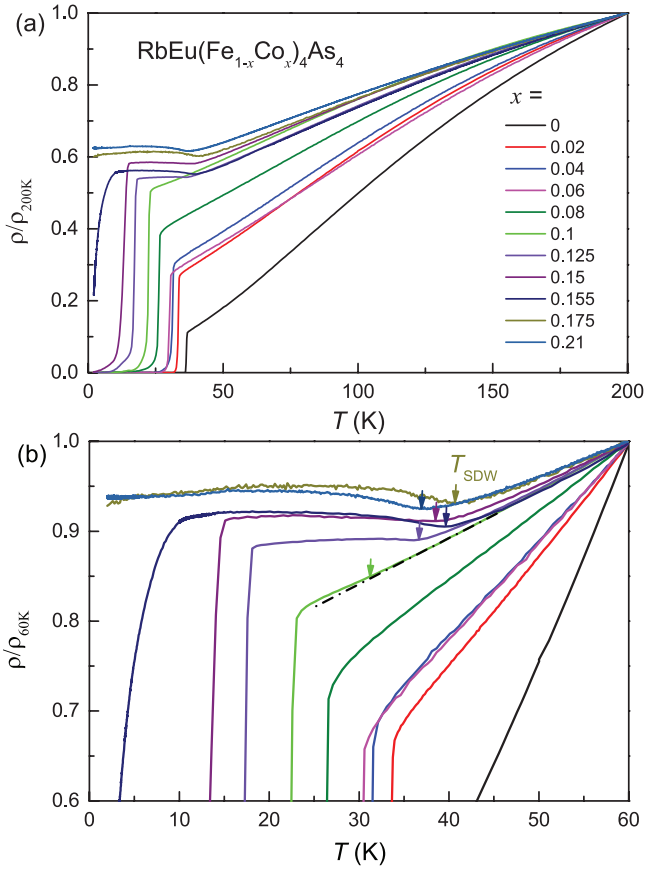

Figure 7. Temperature dependence of resistivity of the $RbEu(Fe_{1-x}Co_x)_4As_4$ polycrystalline samples. The resistivity values were normalized at 200 and 60 K, respectively. T_{SDW} denotes the spin-density-wave ordering temperature.

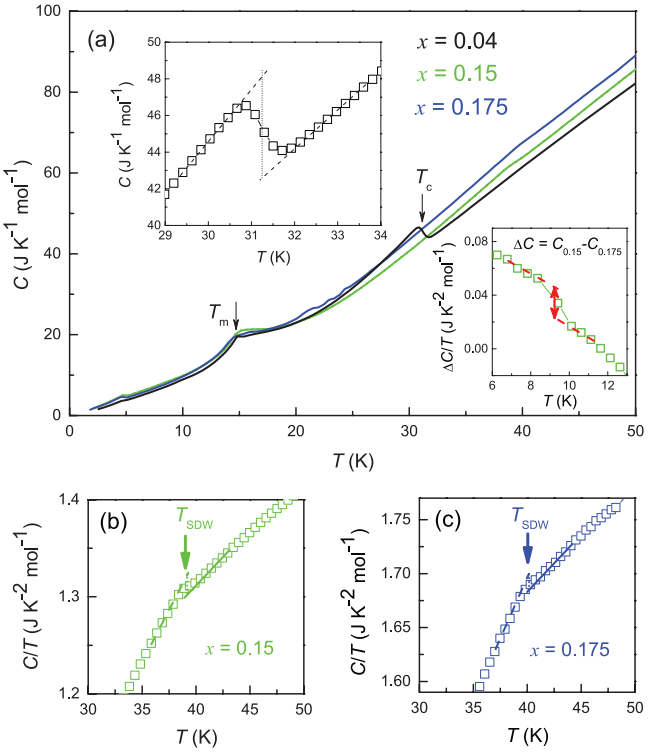

Figure 8. Temperature dependence of specific heat of $RbEu(Fe_{1-x}Co_x)_4As_4$ ($x = 0.04$, 0.15, and 0.175). The right inset of (a) is an expanded plot for $x = 0.04$, and the left inset plots the specific-heat difference (divided by temperature) between the samples of $x = 0.15$ and 0.175, for showing the superconducting transitions. Panels (b) and (c) show the close-ups for the SDW transitions for $x = 0.15$ and 0.175, respectively.

lost at $x \geqslant 0.175$. The T_c^ρ values, determined by the midpoint transition temperature, are coincident with the onset transition temperature, T_c^X, in the magnetic measurement for $x \leqslant 0.1$ (see table 1). However, T_c^ρ is obviously larger than the corresponding T_c^ρ for $x = 0.125$ and 0.15. In addition, the sample of $x = 0.155$ shows a very broad resistive transition, while no signature of the corresponding transition can be detected in the magnetic measurement, as shown in figure 4(h). The higher resistive transition temperature with enhanced transition tails for the SFM suggests a domain-wall SC that was theoretically predicted [37] and experimentally demonstrated in a superconductor-ferromagnet hybrids [38].

Notably, the normal-state resistivity shows an upturn at $T_{SDW} = 30$–40 K for $x \geqslant 0.1$, which is reasonably attributed to the SDW transition that is recovered due to the hole depletion [39]. The hole concentration will be $n_h = 0.25 - x$, if one assumes every Co atom cancels out one hole. Thus, one would expect a monotonic increase of T_{SDW} with Co doping. In reality, however, T_{SDW} shows a maximum of 40 K at $x = 0.175$. The suppression of T_{SDW} can be understood in terms of the Co-induced disorder effect as mentioned above. Similar results were also observed in $RbEu(Fe_{1-x}Ni_x)_4As_4$ [30] and $KCa(Fe_{1-x}M_x)_4As_4$ (M = Co or Ni) [40] systems. Note that, in the latter system, the recovered SDW phase has an interesting hedgehog spin-vortex magnetic structure [41]. It is not clear whether such a magnetic structure is also realized in the Eu-containing 1144-type system.

To confirm the bulk nature of the superconductivity as well as the SDW order, we performed the specific-heat measurements for the $RbEu(Fe_{1-x}Co_x)_4As_4$ samples. As shown in the left inset of figure 8(a), a clear specific-heat jump due to the superconducting transition is seen for $x = 0.04$. However, the expected specific-heat jump for $x = 0.15$ is ambiguous, primarily because the proximity between T_c and T_m. To find out the possible specific-heat anomaly at T_c, we made a subtraction using the $C(T)$ data of the non-superconducting sample with $x = 0.175$ as the background. The result is plotted in the right inset of figure 8(a), which indicates a specific-heat jump with $\Delta C/T = 23$ mJ K^{-2} mol^{-1}. The magnitude of the specific-heat jump is over twice of that of $RbEu(Fe_{0.925}Ni_{0.075})_4As_4$ ($T_c \approx 4$ K) [30] and, comparable to that of $KCa(Fe_{0.951}Ni_{0.049})_4As_4$ ($T_c \approx 10$ K) [40]. Nevertheless, compared with the case of $x = 0.04$, the $\Delta C/T_c$ value is remarkably reduced, which is mainly due to the remarkable decrease of the Sommerfeld coefficient in the underdoped regime [42].

There are also specific-heat anomalies at ~40 K for $x = 0.15$ and 0.175, which are clearly seen in figures 8(b) and (c). The transition is attributed to the recovered SDW ordering, consistent with the resistivity measurement above. Similar observations were reported in $RbEu(Fe_{0.925}Ni_{0.075})_4As_4$ ($T_{SDW} \approx 35$ K) [30] and $KCa(Fe_{0.951}Ni_{0.049})_4As_4$ ($T_{SDW} \approx 52$ K) [40]. As for the Eu-spin ordering, all the samples show a kink at T_m,

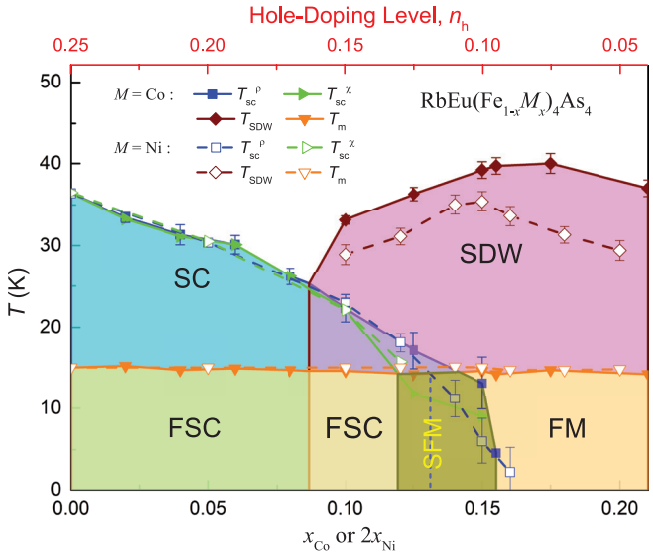

Figure 9. The phase diagram of RbEu(Fe$_{1-x}$Co$_x$)$_4$As$_4$ (solid lines) in comparison with that of RbEu(Fe$_{1-x}$Ni$_x$)$_4$As$_4$ (dashed lines, adapted from [30], © 2017 American Physical Society). T_c^{ρ} and T_c^{χ} denote the superconducting transition temperatures from the resistivity and magnetic measurement, respectively. T_{SDW} and T_m represent the SDW ordering temperature and Eu-spin ordering temperature. FSC and SFM are the abbreviations of 'ferromagnetic superconductor' and 'superconducting ferromagnet'.

instead of a conventional jump. This is probably associated with the quasi-two-dimensional magnetism [24, 43].

4. Concluding remarks

Figure 9 summarizes the Co doping effect on the superconducting and magnetic transitions in RbEu(Fe$_{1-x}$Co$_x$)$_4$As$_4$. The top horizontal axis labels the expected hole concentration, $n_h = 0.25 - x$, in order to address the hole compensation effect. For comparison, the phase diagram of Ni-doped RbEu(Fe$_{1-x}$Ni$_x$)$_4$As$_4$ is superposed with $2x_{Ni}$ as the horizontal axis (because Ni^{2+} has two more itinerant 3*d* electrons than Fe^{2+} does). Upon doping with Co, T_c gradually decreases with the decrease of n_h, and SC finally disappears at $n_h = 0.075$ or $x = 0.175$. At $x \geqslant 0.1$, SDW order recovers, and T_{SDW} increases with the Co doping till $x \geqslant 0.175$. The suppression of SDW order at higher doping regime is attributed to the disorder effect, similar to the case in RbEu(Fe$_{1-x}$Ni$_x$)$_4$As$_4$ [30]. In contrast to the dramatic change associated with the FeAs layers, the magnetic ordering temperature in the Eu layer basically remains unchanged in the whole doping range. Consequently, a superconducting ferromagnet phase is realized in the range of $0.125 \leqslant x \leqslant 0.155$. Overall, the phase diagram is quite similar to that (dashed lines) of Ni-doped system [30]. The slight difference exists on the phase boundaries. The Co-doped system shows higher SDW transition temperatures, suggesting that the disorder effect is relatively weak. The higher T_{SDW} value at $x = 0.125$ corresponds to the lower T_c (possibly due to the competing nature between SC and SDW), which expands the region of SFM phase. Note that this SFM phase extraordinarily shows the coexistence of SC, SDW, and FM.

Finally, we comments on the possible origin of the existence of SFM as well as FSC in the Co-doped RbEuFe$_4$As$_4$ system. As we know, SC and FM are in general antagonistic, making the two phenomena incompatible in a single material [44]. However, the Eu-containing iron-based magnetic superconductors are exceptional due to their multi-orbital characteristic of Fe-3*d* states, which allows both the effective superconducting pairing mainly in the $3d_{yz/zx}$ channels and the RKKY indirect exchange interactions mainly mediated by the $3d_{z^2}$ orbital [1]. The 1144-type system turns out to be the extreme case that SC is simply not suppressed by the Eu^{2+}-spin exchange interactions, which is manifested by the fact that the T_c value of RbEuFe$_4$As$_4$ [18, 19] is even slightly higher than that of its nonmagnetic sister compound CaKFe$_4$As$_4$. Another related experimental fact is that, with the Ca substitution for Eu in RbEuFe$_4$As$_4$, T_c does not change with the decrease of T_m [29]. In this work, we see that the Eu^{2+}-spin ordering does not change with the electron doping, whereas the electronic states in the FeAs layers change essentially. The result can be explained with the above ideas, i.e. different groups of Fe-3*d* orbitals are responsible for SC and FM, respectively [1, 31]. Meanwhile, the SC and FM are decoupled, except for the mutual influence on the compromise configurations (e.g. helical magnetic structure, domain Meissner state, domain vortex-antivortex state, etc). In a word, it is the decoupling nature that both FSC and SFM can be realized in this special system. We hope that future investigations will be able to address how SC and FM compromise especially in the SFM phase.

Acknowledgments

This work was supported by the National Key Research and Development Program of China (Grant No. 2016YFA0300202), the National Natural Science Foundation of China (Grant No. 11474252), and the Fundamental Research Funds for the Central Universities of China (2019FZA3004).

ORCID iDs

Zhi Ren https://orcid.org/0000-0002-3597-1320
Guang-Han Cao https://orcid.org/0000-0002-9669-5761

References

[1] Cao G, Xu S, Ren Z, Jiang S, Feng C and Xu Z 2011 Superconductivity and ferromagnetism in $EuFe_2(As_{1-x}P_x)_2$ *J. Phys.: Condens. Matter* **23** 464204
[2] Zapf S and Dressel M 2017 Europium-based iron pnictides: a unique laboratory for magnetism, superconductivity and structural effects *Rep. Prog. Phys.* **80** 016501
[3] Jiang S, Luo Y, Ren Z, Zhu Z, Wang C, Xu X, Tao Q, Cao G and Xu Z 2009 Metamagnetic transition in $EuFe_2As_2$ single crystals *New J. Phys.* **11** 025007
[4] Xiao Y *et al* 2009 Magnetic structure of $EuFe_2As_2$ determined by single-crystal neutron diffraction *Phys. Rev.* B **80** 174424

[5] Ren Z, Tao Q, Jiang S, Feng C, Wang C, Dai J, Cao G and Xu Z 2009 Superconductivity induced by phosphorus doping and its coexistence with ferromagnetism in $EuFe_2(As_{0.7}P_{0.3})_2$ *Phys. Rev. Lett.* **102** 137002

[6] Jiang S, Xing H, Xuan G, Ren Z, Wang C, Xu Z and Cao G 2009 Superconductivity and local-moment magnetism in $Eu(Fe_{0.89}Co_{0.11})_2As_2$ *Phys. Rev.* B **80** 184514

[7] Jiao W-H, Tao Q, Bao J-K, Sun Y-L, Feng C-M, Xu Z-A, Nowik I, Felner I and Cao G-H 2011 Anisotropic superconductivity in $Eu(Fe_{0.75}Ru_{0.25})_2As_2$ ferromagnetic superconductor *Europhys. Lett.* **95** 67007

[8] Jiao W-H, Zhai H-F, Bao J-K, Luo Y-K, Tao Q, Feng C-M, Xu Z-A and Cao G-H 2013 Anomalous critical fields and the absence of meissner state in $Eu(Fe_{0.88}Ir_{0.12})_2As_2$ crystals *New J. Phys.* **15** 113002

[9] Paramanik U B, Das D, Prasad R and Hossain Z 2013 Reentrant superconductivity in $Eu(Fe_{1-x}Ir_x)_2As_2$ *J. Phys.: Condens. Matter* **25** 265701

[10] Jiao W-H, Liu Y, Tang Z-T, Li Y-K, Xu X-F, Ren Z, Xu Z-A and Cao G-H 2016 Peculiar properties of the ferromagnetic superconductor $Eu(Fe_{0.91}Rh_{0.09})_2As_2$ *Supercond. Sci. Technol.* **30** 025012

[11] Nowik I, Felner I, Ren Z, Cao G H and Xu Z A 2011 Coexistence of ferromagnetism and superconductivity: magnetization and mössbauer studies of $EuFe_2(As_{1-x}P_x)_2$ *J. Phys.: Condens. Matter* **23** 065701

[12] Nowik I, Felner I, Ren Z, Cao G H and Xu Z A 2011 ^{57}Fe and ^{151}Eu mössbauer spectroscopy and magnetization studies of $Eu(Fe_{0.89}Co_{0.11})_2As_2$ and $Eu(Fe_{0.9}Ni_{0.1})_2As_2$ *New J. Phys.* **13** 023033

[13] Jin W T *et al* 2013 Magnetic structure of superconducting $Eu(Fe_{0.82}Co_{0.18})_2As_2$ as revealed by single-crystal neutron diffraction *Phys. Rev.* B **88** 214516

[14] Nandi S, Jin W T, Xiao Y, Su Y, Price S, Shukla D K, Strempfer J, Jeevan H S, Gegenwart P and Brückel T 2014 Coexistence of superconductivity and ferromagnetism in P-doped $EuFe_2As_2$ *Phys. Rev.* B **89** 014512

[15] Nandi S *et al* 2014 Coexistence of ferromagnetism and superconductivity in iron based pnictides: a time resolved magnetooptical study *Phys. Rev.* B **90** 094407

[16] Jin W T *et al* 2015 Magnetic ground state of superconducting $Eu(Fe_{0.88}Ir_{0.12})_2As_2$: a combined neutron diffraction and first-principles calculation study *Phys. Rev.* B **91** 064506

[17] Ren Z, Lin X, Tao Q, Jiang S, Zhu Z, Wang C, Cao G and Xu Z 2009 Suppression of spin-density-wave transition and emergence of ferromagnetic ordering of Eu^{2+} moments in $EuFe_{2-x}Ni_xAs_2$ *Phys. Rev.* B **79** 094426

[18] Kawashima K, Kinjo T, Nishio T, Ishida S, Fujihisa H, Gotoh Y, Kihou K, Eisaki H, Yoshida Y and Iyo A 2016 Superconductivity in Fe-based compound $EuAFe_4As_4$ (A = Rb and Cs) *J. Phys. Soc. Japan* **85** 064710

[19] Liu Y *et al* 2016 Superconductivity and ferromagnetism in hole-doped $RbEuFe_4As_4$ *Phys. Rev.* B **93** 214503

[20] Liu Y, Liu Y-B, Chen Q, Tang Z-T, Jiao W-H, Tao Q, Xu Z-A and Cao G-H 2016 A new ferromagnetic superconductor: $CsEuFe_4As_4$ *Sci. Bull.* **61** 1213–20

[21] Smylie M P *et al* 2018 Anisotropic superconductivity and magnetism in single-crystal $RbEuFe_4As_4$ *Phys. Rev.* B **98** 104503

[22] Albedah M A, Nejadsattari F, Stadnik Z M, Liu Y and Cao G-H 2018 Mössbauer spectroscopy measurements on the 35.5 K superconductor $Rb_{1-\delta}EuFe_4As_4$ *Phys. Rev.* B **97** 144426

[23] Albedah M A, Nejadsattari F, Stadnik Z M, Liu Y and Cao G-H 2018 Magnetism of the 35 K superconductor $CsEuFe_4As_4$ *J. Phys.: Condens. Matter* **30** 155803

[24] Willa K, Willa R, Bao J-K, Koshelev A E, Chung D Y, Kanatzidis M G, Kwok W-K and Welp U 2019 Strongly fluctuating moments in the high-temperature magnetic superconductor $RbEuFe_4As_4$ *Phys. Rev.* B **99** 180502

[25] Vlasko-Vlasov V K, Koshelev A E, Smylie M, Bao J-K, Chung D Y, Kanatzidis M G, Welp U and Kwok W-K 2019 Self-induced magnetic flux structure in the magnetic superconductor $RbEuFe_4As_4$ *Phys. Rev.* B **99** 134503

[26] Iida K *et al* 2019 Coexisting spin resonance and long-range magnetic order of Eu in $EuRbFe_4As_4$ *Phys. Rev.* B **100** 014506

[27] Devizorova Z and Buzdin A 2019 Superconductivity-driven helical magnetic structure in $EuRbFe_4As_4$ ferromagnetic superconductor *Phys. Rev.* B **100** 104523

[28] Iyo A, Kawashima K, Kinjo T, Nishio T, Ishida S, Fujihisa H, Gotoh Y, Kihou K, Eisaki H and Yoshida Y 2016 New-structure-type Fe-based superconductors: $CaAFe_4As_4$ (A = K, Rb, Cs) and $SrAFe_4As_4$ (A = Rb, Cs) *J. Am. Chem. Soc.* **138** 3410–5

[29] Kawashima K *et al* 2018 Superconducting state in $Eu_{1-x}Ca_xRbFe_4As_4$ with 1144-type structure *J. Phys.: Conf. Ser.* **969** 012027

[30] Liu Y, Liu Y B, Yu Y-L, Tao Q, Feng C-M and Cao G-H 2017 $RbEu(Fe_{1-x}Ni_x)_4As_4$: From a ferromagnetic superconductor to a superconducting ferromagnet *Phys. Rev.* B **96** 224510

[31] Xu C C, Chen Q J and Cao C 2019 Unique crystal field splitting and multiband RKKY interactions in Ni-doped $EuRbFe_4As_4$ *Commun. Phys.* **2** 16

[32] Lorenz B and Chu C-W 2005 Superconducting ferromagnets: ferromagnetic domains in the superconducting state *Nat. Mater.* **4** 516–7

[33] Wang Z-C, Liu Y, Wu S-Q, Shao Y-T, Ren Z and Cao G-H 2019 Giant anisotropy in superconducting single crystals of $CsCa_2Fe_4As_4F_2$ *Phys. Rev.* B **99** 144501

[34] Jiao W-H, Tao Q, Ren Z, Liu Y and Cao G-H 2017 Evidence of spontaneous vortex ground state in an iron-based ferromagnetic superconductor *npj Quantum Mater.* **2** 50

[35] Paulsen C, Hykel D J, Hasselbach K and Aoki D 2012 Observation of the Meissner–Ochsenfeld effect and the absence of the meissner state in UCoGe *Phys. Rev. Lett.* **109** 237001

[36] Stolyarov V S *et al* 2018 Domain meissner state and spontaneous vortex-antivortex generation in the ferromagnetic superconductor $EuFe_2(As_{0.79}P_{0.21})_2$ *Sci. Adv.* **4** 1061

[37] Buzdin A I and Mel'nikov A S 2003 Domain wall superconductivity in ferromagnetic superconductors *Phys. Rev.* B **67** 020503

[38] Yang Z, Lange M, Volodin A, Szymczak R and Moshchalkov V V 2004 Domain-wall superconductivity in superconductor ferromagnet hybrids *Nat. Mater.* **3** 793–8

[39] Zinth V, Dellmann T, Klauss H-H and Johrendt D 2011 Recovery of a parentlike state in $Ba_{1-x}K_xFe_{1.86}Co_{0.14}As_2$ *Angew. Chem. Inter. Ed.* **50** 7919–23

[40] Meier W R *et al* 2018 Hedgehog spin-vortex crystal stabilized in a hole-doped iron-based superconductor *npj Quantum Mater.* **3** 5

[41] Kreyssig A *et al* 2018 Antiferromagnetic order in $CaK(Fe_{1-x}Ni_x)_4As_4$ and its interplay with superconductivity *Phys. Rev.* B **97** 224521

[42] Hardy F *et al* 2016 Strong correlations, strong coupling, and s-wave superconductivity in hole-doped $BaFe_2As_2$ single crystals *Phys. Rev.* B **94** 205113

[43] Willa K, Smylie M P, Bao J-K, Chung D Y, Kanatzidis M G, Kwok W-K and Welp U 2019 Magnetic and superconducting anisotropy in Ni-doped $RbEuFe_4As_4$ single crystals (arXiv:1908.00773)

[44] Bulaevskii L N, Buzdin A I, Kulić M L and Panjukov S V 1985 Coexistence of superconductivity and magnetism theoretical predictions and experimental results *Adv. Phys.* **34** 175–261